Bulletin of the Seismological Society of America, Vol. 97, No. 5, pp. 1432–1448, October 2007, doi: 10.1785/0120050204

Ⓔ

Seismic Amplification within the Seattle Basin, Washington State: Insights from SHIPS Seismic Tomography Experiments

by Catherine M. Snelson,* Thomas M. Brocher, Kate C. Miller, Thomas L. Pratt, and Anne M. Tréhu

Abstract Recent observations indicate that the Seattle sedimentary basin, underlying Seattle and other urban centers in the Puget Lowland, Washington, amplifies long-period (1–5 sec) weak ground motions by factors of 10 or more. We computed east-trending *P*- and *S*-wave velocity models across the Seattle basin from Seismic Hazard Investigations of Puget Sound (SHIPS) experiments to better characterize the seismic hazard the basin poses. The 3D tomographic models, which resolve features to a depth of 10 km, for the first time define the *P*- and *S*-wave velocity structure of the eastern end of the basin. The basin, which contains sedimentary rocks of Eocene to Holocene, is broadly symmetric in east–west section and reaches a maximum thickness of 6 km along our profile beneath north Seattle. A comparison of our velocity model with coincident amplification curves for weak ground motions produced by the 1999 Chi-Chi earthquake suggests that the distribution of Quaternary deposits and reduced velocity gradients in the upper part of the basement east of Seattle have significance in forecasting variations in seismic-wave amplification across the basin. Specifically, eastward increases in the amplification of 0.2- to 5-Hz energy correlate with locally thicker unconsolidated deposits and a change from Crescent Formation basement to pre-Tertiary Cascadia basement. These models define the extent of the Seattle basin, the Seattle fault, and the geometry of the basement contact, giving insight into the tectonic evolution of the Seattle basin and its influence on ground shaking.

Online material: Seismic velocity depth slices and data.

Introduction

The tectonic setting of the Pacific Northwest is dominated by oblique subduction of the Juan de Fuca plate beneath the North American plate (e.g., Riddihough, 1984; Monger and Nokleberg, 1996). This oblique plate convergence results in north–south shortening (Khazaradze *et al.*, 1999), such that both dextral strike-slip faults and east-trending thrust faults have formed in the Puget Lowland fore-arc basin (e.g., Johnson *et al.*, 1996; Pratt *et al.*, 1997; Wells *et al.*, 1998). Crustal faulting in the Puget Lowland has been accompanied by the formation of a series of thick, fault- or fold-bounded sedimentary basins beneath many of the urban centers in the region (Finn, 1990; Brocher *et al.*, 2001). Of these, the Seattle basin underlies the greatest population, including the cities of Seattle, Bremerton, and Bellevue, Washington. The Seattle basin is also bounded to the south by the Seattle fault, which provides a source zone for potentially large earthquakes directly beneath these cities (Johnson *et al.*, 1994; Pratt *et al.*, 1997; Nelson *et al.*, 2003). Ominously, the Seattle basin also has been documented to substantially amplify long-period seismic waves (e.g., Frankel *et al.*, 1999, 2002; Pratt *et al.*, 2003a; Barberopoulou *et al.*, 2004, 2006; Pratt and Brocher, 2006). In this article, we use tomographic analyses of seismic data to examine the geometry and velocity structure of the Seattle basin and its influence on ground motions.

We use data from Seismic Hazard Investigations of Puget Sound (SHIPS) projects, a series of studies designed specifically to help characterize the seismic hazard in the region. There have been five SHIPS experiments to date: "Wet" SHIPS in 1998 (Fisher *et al.*, 2000); "Dry" SHIPS in 1999 (Brocher *et al.*, 2000a, b); "Kingdome" SHIPS in 2000 (Brocher *et al.*, 2000a, 2002); "Seattle" SHIPS in 2002 (Pratt *et al.*, 2003b); and "Bellingham" SHIPS in 2002 (Brocher *et al.*, 2003). The 1999 and 2000 experiments were designed to study the Seattle basin, and it is those data we analyze here. We conducted the "Dry" SHIPS experiment (Fig. 1) in

*Present address: Department of Earth and Environmental Science, New Mexico Institute of Mining and Technology, Socorro, New Mexico 87801.

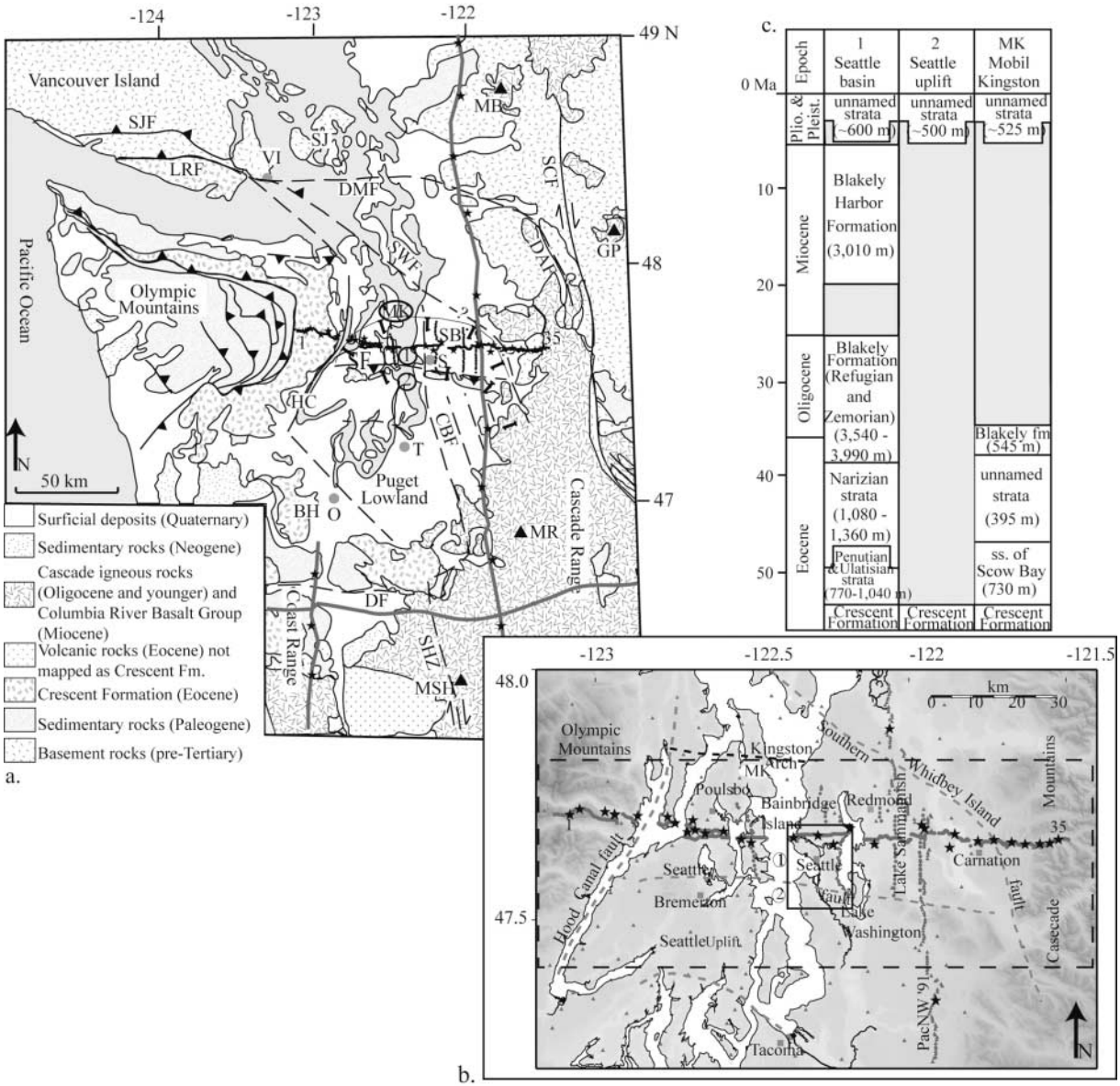

Figure 1. (a) Generalized geologic map of western Washington State (modified from Johnson *et al.*, 1999). Seismic stations for "Dry" SHIPS are the small black dots and shot points are the small stars. Abbreviations for cities: S, Seattle; T, Tacoma; O, Olympia; VI, Victoria. Circled 1, 2, and MK are stratigraphic column locations. Abbreviations for geologic features (fault, heavy lines, dashed where inferred; volcanoes, triangles): BH, Black Hills; CBF, Coast Range Boundary fault; DAF, Darrington fault; DF, Doty fault; DMF, Devils Mountain fault; GP, Glacier Peak; HC, Hood Canal fault; LRF, Leech River fault; MA, Mt. Adams; MB, Mt. Baker; MR, Mt. Rainer; MSH, Mt. St. Helens; SB, Seattle Basin; SCF, Straight Creek fault; SF, Seattle fault; SHZ, Saint Helens zone; SJ, San Juan Islands; SJF, San Juan fault; SWF, Southern Whidbey Island fault. (b) Topographic base map of study area. Darker shades of gray represent higher elevations. The 1999 SHIPS profile is indicated by gray dots (receiver stations) and stars (shot points). The 2000 SHIPS profile is represented by a square where 206 seismic recorders were placed 1 km apart throughout the grid. Shots were nominally placed at the corners of the grid and at the center (Kingdome sports area implosion). The PacNW 1991 seismic refraction profile is defined by the small gray triangles trending north–south and the shot points are the stars along the north–south-trending profile (Miller *et al.*, 1997). Major faults are indicated by dashed gray lines. Cities are in italics. Tomography model area is shown by the large dashed box. (c) Stratigraphic column for the Puget Lowland. Shaded areas are intervals of nondeposition and/or erosion (modified from Johnson *et al.*, 1994, 1996).

September 1999 to better define the east–west geometry of the Seattle basin and to determine the velocity structure of the Cenozoic sedimentary basin fill. The March 2000 SHIPS experiment recorded data during the Kingdome sports arena implosion in downtown Seattle, as well as four small blasts (Fig. 1) ("Kingdome" SHIPS).

In this article, we present results of our tomographic analysis of data acquired during "Dry" and "Kingdome" SHIPS. The results provide a picture for the entire Seattle basin unlike previous surveys. The *P*-wave velocity model provides new constraints on the eastern margin of the Seattle basin, and we have generated the first *S*-wave velocity model across the basin. These results have provided new insight into the amplification and attenuation within the Seattle basin. In addition, these models define the contact between the two basement terranes, giving insight into the tectonic evolution of the Seattle basin and its influence on ground shaking.

Geologic Background

During early Paleogene (~50 Ma); Paleocene to mid-Eocene basaltic and sedimentary rocks of the Crescent Formation (Siletz volcanic terrane) were accreted to western North America (Tabor and Cady, 1978; Johnson, 1984, 1985; Atwater, 1989; Burchfiel *et al.*, 1992). The Crescent Formation now forms the basement rocks of western Washington State, including the Puget Lowland, and acts as a backstop for the accumulation of the accretionary wedge (Fig. 1) (e.g., Tabor and Cady, 1978; Atwater, 1989; Brandon and Calderwood, 1990; Brandon and Vance, 1992). Crescent Formation rocks underlying the western side of the Puget Lowland are in contact with pre-Tertiary Cascade volcanic rocks beneath the eastern side of the Lowland (Tabor and Cady, 1978; Johnson, 1984, 1985; Atwater, 1989). The location of this basement contact is not well defined, but the velocity and density contrast between the basement rocks likely influences basin geometry and potential seismic-wave amplification (e.g., Finn, 1990; Pratt *et al.*, 2003a).

Crescent Formation basement rocks are compressed in a series of folds and faults that form uplifted blocks and down-dropped basins beneath the Puget Lowland. The most prominent of these uplifted blocks, the Seattle uplift, lies immediately south of the Seattle basin and is bounded by the Seattle and Tacoma fault zones (Fig. 1) (Pratt *et al.*, 1997; Brocher *et al.*, 2001, 2004; Johnson *et al.*, 2004; Sherrod *et al.*, 2004).

The stratigraphy within the Seattle basin is known from surface exposures, industry boreholes, and seismic-reflection profiles tied to the boreholes (Fig. 1c) (Johnson *et al.*, 1994, 1999; Brocher and Ruebel, 1998; Rau and Johnson, 1999). As much as 1.1 km of unconsolidated, primarily Quaternary and Holocene deposits (Jones, 1996) form the top of the basin and are thought to be the main contributor to the amplification of seismic energy (Frankel *et al.*, 1999, 2002; Pratt *et al.*, 2003a; Barberopoulou *et al.*, 2004, 2006; Pratt and Brocher, 2006). The upper portions of the unconsolidated deposits are a temporally and spatially complex stratigraphy of glacial outwash, till, lacustrine, and recessional deposits formed when the Lowland was glaciated at least six different times in the Pleistocene (Booth, 1994). Well logs and seismic-reflection data indicate that these Quaternary and Holocene deposits overlie sedimentary rocks of Eocene to Miocene (Fig. 1c). The remaining stratigraphy is here summarized from Johnson *et al.* (1994, 1996), Jones (1996), Brocher and Ruebel (1998), and Rau and Johnson (1999) (Fig. 1c). The Miocene Blakely Harbor Formation consists of nonmarine sandstone, conglomerate, and siltstone. The conglomerate clasts are poorly sorted, well-rounded pebbles, cobbles, and boulders of which ~85% are from the Crescent Formation. This formation marks the motion of the Seattle fault in the early Miocene (ten Brink *et al.*, 2002). The Eocene to Oligocene Blakeley Formation consists of various deep marine sequences. The Refugian and Zemorian of the Blakeley Formation consist of siltstone, claystone, and minor sandstone. Tuffaceous interbeds and rare macerated carbonaceous material are common. Forams suggest an upper bathyal depositional environment. The Narizian strata consist of sandstone and siltstone; claystone and tuffaceous interbeds are common. The depositional environment is interpreted as upper bathyal depths. Penutian and Ulatisian strata consist of siltstone and claystone with interbeds of tuff and very fine grained to granular sandstone. The depositional environment is interpreted as middle bathyal depths. The Crescent Formation consists of basalt and minor interbeds of siltstone, tuff, and conglomerate. The depositional environment suggests neritic depths.

The Seattle fault zone bounds the Seattle basin to the south and consists of several east–west-trending faults (Johnson *et al.*, 1999; Blakely *et al.*, 2002). Motion on the Seattle fault has caused a north–south asymmetry to the Seattle basin, wherein the basin thins from 7 to 10 km near the fault to about 2.5 km at its northern end (Johnson *et al.*, 1994; Pratt *et al.*, 1997; Brocher *et al.*, 2001, 2004; ten Brink *et al.*, 2002; Van Wagoner *et al.*, 2002). The western end of the Seattle fault zone is thought to lie at the east edge of the Olympic Mountains, whereas the eastern end of the fault is interpreted to lie near the base of the Cascade Range near the southeast projection of the Southern Whidbey Island fault (Gower *et al.*, 1985; Finn, 1990; Johnson *et al.*, 1994, 1996; Pratt *et al.*, 1997; Brocher *et al.*, 2001).

Several large crustal earthquakes ruptured the Puget Lowland during the late Holocene (Bucknam *et al.*, 1992; Haugerud *et al.*, 2003; Nelson *et al.*, 2003; Sherrod *et al.*, 2004). The best documented of these occurred about 1000 to 1100 years ago on the Seattle fault, causing 7 m of uplift, fault scarps, a tsunami, and landslides (Atwater and Moore, 1992; Bucknam *et al.*, 1992; Schuster *et al.*, 1992; Nelson *et al.*, 2003). This evidence suggests that the Seattle fault zone can produce M 7.0+ earthquakes (Bucknam *et al.*, 1992; Pratt *et al.*, 1997).

Previous Geophysical Studies

Potential Field Geophysics

Daneš *et al.* (1965) first reported the Seattle basin on the basis of a pronounced low gravity. Gower *et al.* (1985) delineated several linear features in gravity and magnetic data associated with inferred or known crustal faults in the Puget Lowland, including the Olympia, Tacoma, and Seattle faults. More recent assessments of crustal fault geometry have tied magnetic and gravity data to geologic mapping and interpretations of seismic-reflection data (e.g., Finn, 1990; Pratt *et al.*, 1997; Blakely *et al.*, 2002). Simultaneous inversions of gravity data and tomography models from the 1998 SHIPS experiment have refined the subsurface picture of the Seattle fault and Seattle basin (Brocher *et al.*, 2001; Parsons *et al.*, 2001; ten Brink *et al.*, 2002), although these models lack the data to define the eastern portion of the Seattle basin, the length of the Seattle fault, and the extent of the Crescent Formation (Siletz) basement rocks in the subsurface.

Earthquake Studies

Earthquake tomography studies show that higher-velocity rocks, interpreted as Crescent Formation basement, extend to about 20 to 30 km depth under the Puget Sound (Lees and Crosson, 1990; Symons and Crosson, 1997; Van Wagoner *et al.*, 2002). Schultz and Crosson (1996) determined that the crustal thickness in the Puget Lowland is about 35 km. Although earthquake studies have yielded valuable regional structural information, they have not defined the contact between the Eocene Crescent Formation and Pre-Tertiary (mainly Eocene) Cascade basement rocks beneath the Puget Lowland.

Controlled-Source Seismic Studies

A series of crustal-scale studies have recently been conducted in the Puget Lowland using seismic reflection and refraction profiling. Reinterpretation of industry seismic-reflection data have led to a working hypothesis that the Puget Lowland rides on a north-verging décollement at about 20 km depth (Pratt *et al.*, 1997).

In 1991, a south-trending seismic-refraction profile (Fig. 1) crossed the Puget Lowland along the Cascade front (Miller *et al.*, 1997), providing cross-line constraint on the eastern edge of the "Dry" SHIPS profile. Data from a 1995 east-trending line located south of the Seattle basin (Fig. 1) imaged the suture zone between the Crescent Formation and the Pre-Tertiary basement rocks (Parsons *et al.*, 1999).

A tomographic model from 1998 SHIPS provided a detailed image for much of the Puget Lowland to a depth of ~11 km (Brocher *et al.*, 2001). The velocity model showed that the Seattle basin is about 7 to 10 km deep and that the basin is asymmetric in the north–south direction (Brocher *et al.*, 2001). In this model, the Seattle basin appears to be asymmetric in the east–west direction, probably a result of lack of coverage in the eastern edge of the model (Brocher *et al.*, 2001). The 1998 SHIPS experiment did not define the contact between the Crescent Formation and Pre-Tertiary Cascade basement rocks.

It is necessary to define this basement contact at the east edge of the Crescent Formation to understand where the crustal earthquakes are generated. Are they generated at the interface between the Crescent Formation and the Cascadia rocks? Or are the earthquakes generated in the highly fractured Crescent Formation? The location of the potential hypocenter may have direct implications to the amount of ground shaking that will occur.

Data Acquisition and Analysis

Acquisition

The 1999 SHIPS seismic-refraction line crossed the Seattle basin in an east–west direction. The profile was ~117 km in length, and extended from the Olympic Mountains, through north Seattle, to the foothills of the Cascades (Fig. 1b). Four shorter and less densely instrumented cross-lines provide constraints on the shallow, three-dimensional structure of the eastern side of the basin.

During the 1999 SHIPS experiment (Brocher *et al.*, 2000a), 1008 seismometers were installed along the lines with a nominal spacing of 100 m. To record shear waves, 239 of our instruments were three-component recorders distributed nominally at 400-m spacing. For sources, we detonated 38 shots at 29 sites, with a nominal spacing of 4 km and charge sizes ranging from 11 to 1136 kg. Overall, the data quality was good to high (Fig. 2).

The March 2000 "Kingdome" SHIPS experiment was designed to study the site response and the velocity structure within the upper 2 km of the Seattle basin (Brocher *et al.*, 2000b, 2002). We deployed a hexagonal grid of 206 seismic recorders within the city of Seattle (Fig. 1b, box) with a nominal station spacing of about 1 km. In addition to recording the implosion of the Kingdome sports arena for site-response analysis, we detonated four 68-kg shots at the corners of the grid for shallow tomographic analysis. These data were poor to good quality because of the reverberatory nature of an implosion. In addition, the four corner shots were not very impulsive, thereby only providing data near source and not across the grid.

Analysis

We derived velocity models from the combined 1999 and 2000 SHIPS data by using the 3D tomographic method of Hole (1992). Important parameters included the choice to implement the code in 3D, the starting 1D velocity model, and the smoothing schedule for updating velocity models. We chose a 3D approach because of the crooked-line geometry of the 1999 SHIPS profile (Fig. 1). Our 3D model space was 137 km in length (east–west) by 51 km wide (north–south) and 40 km deep with a 400-m grid spacing

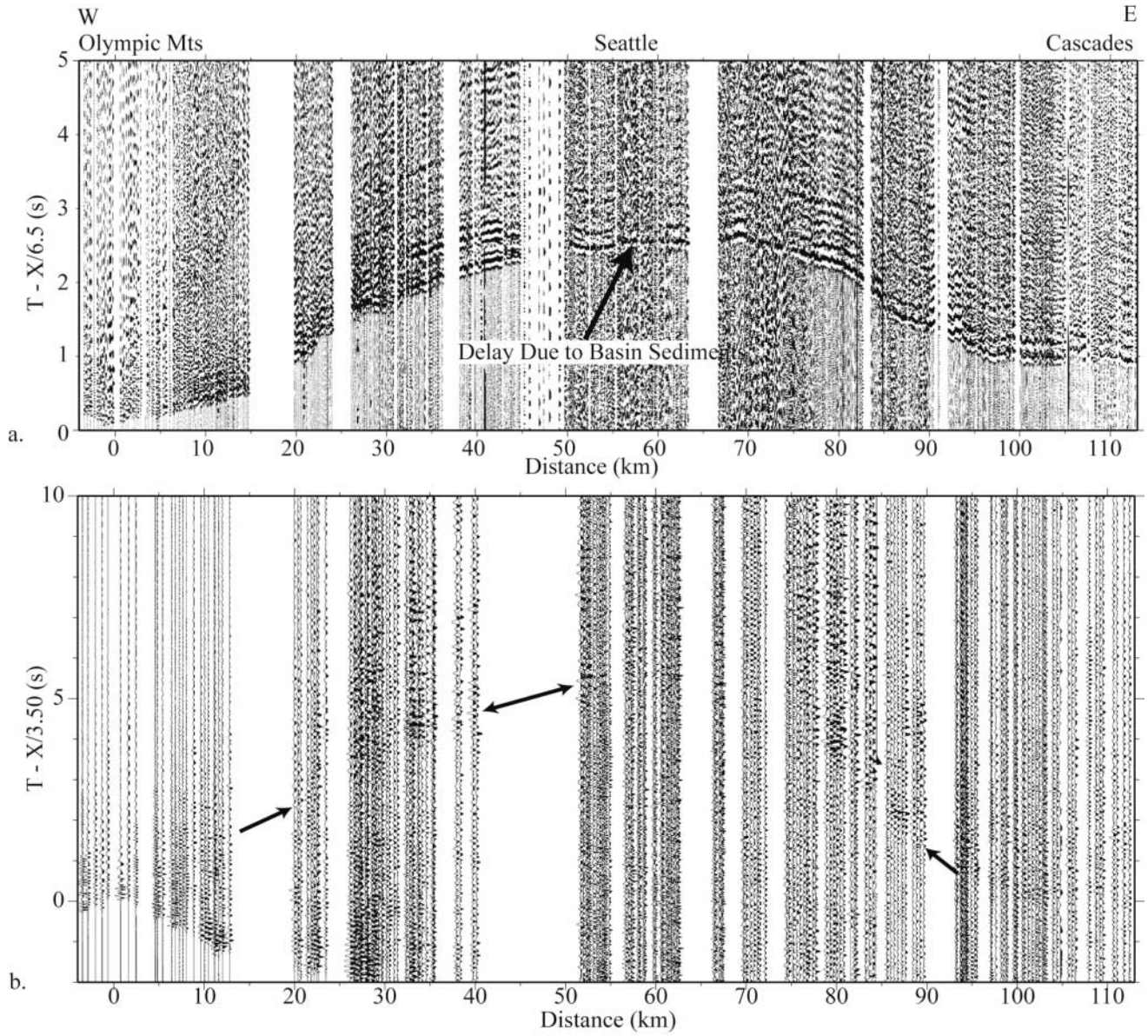

Figure 2. Record sections from shot point 1 at the west end of the profile as seen in Figure 1b. (a) *P*-wave seismic-record section. Note that the Seattle basin is distinguished by a 2-sec travel-time delay due to basin sediments. These data have a Butterworth bandpass filter applied and are reduced at 6.5 km/sec. (b) An *S*-wave seismic-record section from the east–west direction. Arrows note the *S*-wave arrivals. The data quality is not as high as the *P*-wave data. These data have a Butterworth bandpass filter applied and are reduced at 3.5 km/sec.

(Fig. 1b, dashed rectangle). We present 2D velocity models and hit counts (number of rays/cell) derived from our 3D grid. Because there should be low hit counts in the cells where there were no picks, we chose to collapse the 3D velocity model into a 2D velocity slice. We did this by weighting model values by the hit count and then summing in the north–south direction, which produced a summary image versus a series of partial slices. We did not include the cross-line data for these purposes. (Ⓔ See E1–E3 in the electronic edition of BSSA.)

The initial 3D, *P*-wave velocity model was an expansion of a 1D velocity model compiled from *a priori* information for the study area utilizing the previous *P*-wave velocity models of the Seattle basin (e.g., Parsons *et al.*, 1999; Hiett, 2000; Brocher *et al.*, 2001). Our assumption in utilizing these data was that we would more likely converge faster to the final model. We derived our final *P*-wave model from the inversion of more than 13,000 *P*-wave first-arrival travel-time picks. We estimate the travel-time picking error for the first arrivals to be ~0.1 sec in high signal-to-noise ratio por-

tions of the seismic data, and ~0.15 sec otherwise. Our starting model produced a root mean square (rms) error of 1.34 sec. We carried out three runs of ten iterations each to produce the final model. The first and second runs used a smoothing factor of 40 × 40 × 20 grid nodes (16 km × 16 km × 8 km) and 30 × 30 × 10 grid nodes (12 km × 12 km × 4 km), respectively. The final run used a smoothing factor of 20 × 20 × 10 grid nodes (8 km × 8 km × 4 km) and produced a model with an rms error equal to the estimated picking error of ~ 0.1 sec. A detailed examination of the fit between observed and calculated travel times shows that there are places where the misfit is much less than 0.1 sec, as well as places where it is as large as 0.2 sec (Fig. 3a).

First-arrival times for over 1500 arrivals were inverted for the *S*-wave velocity model. The quality of the *S*-wave arrivals on the horizontal component data is fair to good, and several of the 1999 shots produced obvious shear-wave arrivals across the entire length of the profile (Fig. 2b). Many shots recorded on the horizontal components are highly reverberatory, which made picking the *S*-wave arrivals difficult. In particular, there is a lack of short offset data in the central portion of the profile due to the poor signal-to-noise ratio (i.e., the city of Seattle). To address some of this problem, the *P*-wave first-arrival times were converted to approximate *S*-wave arrival times assuming a Poisson's ratio of 1.8 and then used as a guide for picking *S*-wave arrivals. This approach worked as a first-order approximation. The initial *S*-wave velocity model was converted from the final *P*-wave model by using a V_p/V_s ratio of 1.8, which is appropriate for basement rocks in the study area (Brocher and Christensen, 2001). The *S*-wave arrivals were then inverted using the 3D approach described by Hole (1992). The smoothing strategy was the same as the *P*-wave velocity model. The initial *S*-wave velocity model had a 1-km-grid cell spacing. The final rms error for the *S*-wave model is 0.2 sec, which is comparable to our estimate of the picking error for these arrivals (Fig. 3b).

A sense of the spatial resolution of the *P*- and *S*-wave velocity models can be obtained by jointly examining the rms error, travel-time fits, hit count, and checkerboard tests. Unfortunately, the nonlinear technique we used does not produce a resolution matrix (Hole, 1992). The number of rays that intersect (hit) any given cell provides an estimate of the resolution in that cell. Overall, the ray coverage is adequate throughout the *P*-wave velocity model, with a minimum of 5 hits and a maximum of 1884 hits per cell, whereas the hit count for the *S*-wave model reaches a maximum 420 hits per cell (Fig. 4). The ray coverage is especially dense where shots were fired twice at the same location. Ray coverage from the 1999 SHIPS cross-lines and 2000 SHIPS data was adequate in the upper 2 km, but decreased rapidly below that depth (Snelson, 2001). Because the southwest corner shot in the 2000 SHIPS experiment was not well recorded, the southern portion of the grid, which crossed the Seattle fault, provides limited ray coverage. The maximum depth of ray penetration is 16 km for the *P*-wave velocity model and 24 km for the *S*-wave velocity model. The lack of near-source data does result in a velocity trade-off with depth.

Following the resolution test method of Zelt (1998), we ran three separate checkerboard tests using different-size checkers. The first 2D checkerboard used 15 km × 15 km sinusoidal checkers with amplitudes of ±3% added to the final *P*-wave velocity model. Travel times from this model were calculated to serve as "observed" travel times in an inversion run that the final model was input. The inversion was then allowed to run for five iterations. Subsequent runs used 10 km × 10 km and 5 km × 5 km sinusoidal checkers with amplitudes of ±3%. The shapes of the checkers above 7 km depth were well recovered with the 15 km checkers (Fig. 5a), and those above 4 km depth were recovered with 10-km checkers (Fig. 5b). We could not adequately recover the 5-km checkers (Fig. 5c). This is consistent with the data set, where there are minimal data due to survey design above 2 km in the model. These results suggest that the best resolution is from 2 to 7 km depth in the model (Fig. 5), which is sufficient for imaging the base of the Seattle basin.

Results

Seattle Basin Geometry

Our tomography results show that in east–west profile, the Seattle basin is a nearly symmetric, bowl-shaped region of low-velocity (1.7–4.5 km/sec) rocks and sediments with sides sloping about 20° on the east and 29° on the west (Fig. 6) and see Ⓔ E1–E5 in the electronic edition of BSSA. As explained subsequently, we interpret the bottom of the sedimentary basin to be at or near the 4.5 km/sec contour on the *P*-wave velocity model. The length of the Seattle basin on our profile is ~76 km measured from where the 4.5 km/sec contour comes within 1 km of the surface at each end (Fig. 6 and Ⓔ E1–E5 in the electronic edition of BSSA). The maximum basin thickness along our profile is about 6 km, which is consistent with the profile's location several kilometers to the north of the thickest (~7–10 km thick) part of the basin as interpreted from north–south-trending seismic-reflection profiles (Johnson *et al.*, 1994; ten Brink *et al.*, 2002), gravity, and 3D tomographic models (Brocher *et al.*, 2001; Van Wagoner *et al.*, 2002). The eastern edge of the basin lies near the interpreted southeast projection of the Southern Whidbey Island fault (Johnson *et al.*, 1996). The western edge lies near the hypothesized Hood Canal-Discovery Bay fault (Gower *et al.*, 1985; Johnson *et al.*, 1994). Neither end of the basin shows an abrupt step consistent with significant displacement by a fault, although a small (<0.5 km) step would be below the resolution of our model.

Our profile ties the north-trending, 1998 SHIPS seismic-reflection line at 52 km at Puget Sound (Fig. 6) (Ⓔ E1–E5 in the electronic edition of BSSA; ten Brink *et al.*, 2002), which is in turn tied to the Mobil-Kingston #1 well. In the

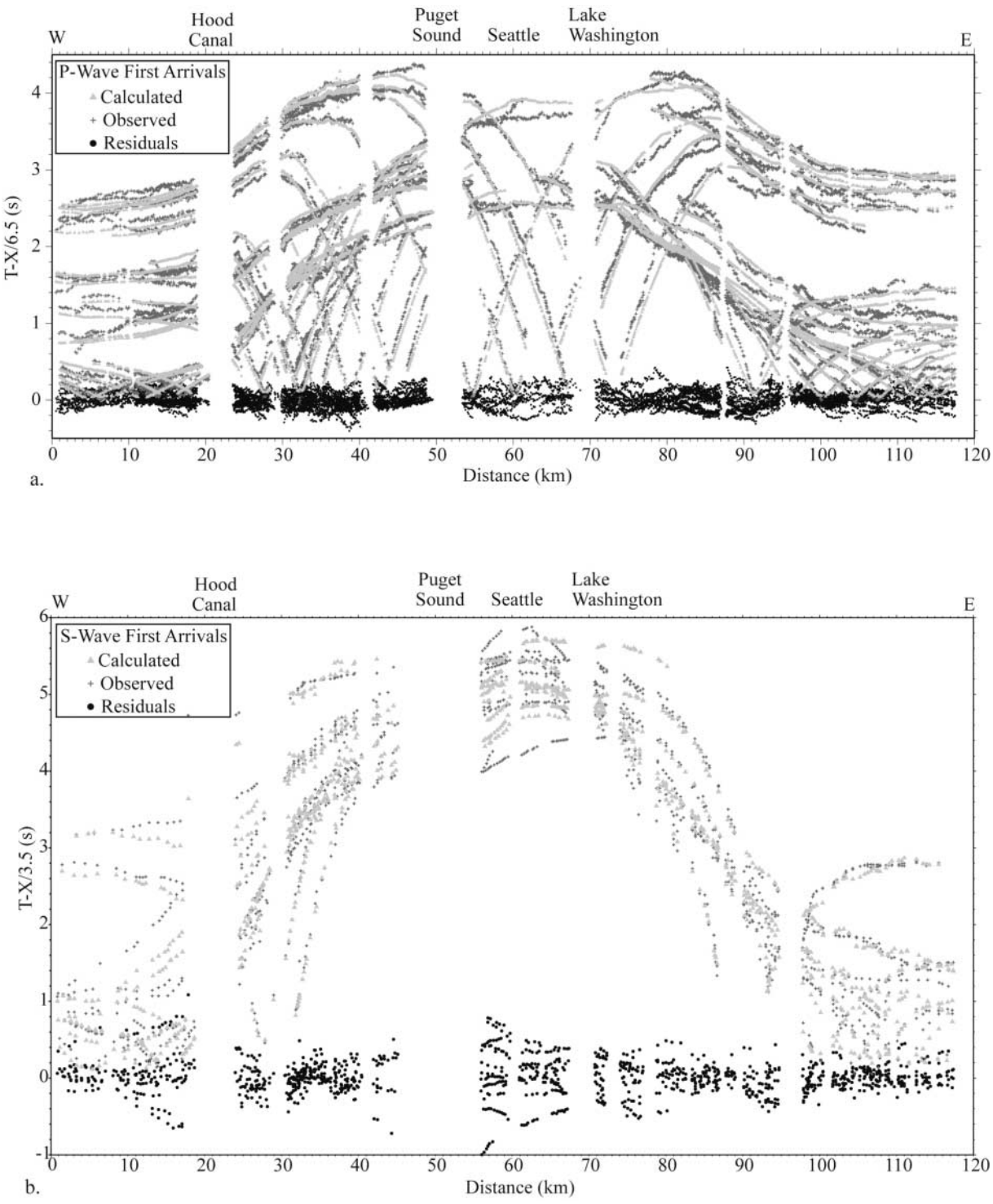

Figure 3. (a) *P*-wave travel-time fits for the 1999 SHIPS data. Travel times are reduced at 6.5 km/sec. Plus signs are the observed travel times, triangles are the calculated travel times from the inversion, and the dots are the residuals or difference between the observed and calculated travel times. (b) *S*-wave travel-time fits for the 1999 SHIPS data. Travel times are reduced at 3.5 km/sec. Plus signs are the observed travel times, triangles are the calculated travel times from the inversion, and the dots are the residuals or difference between the observed and calculated travel times.

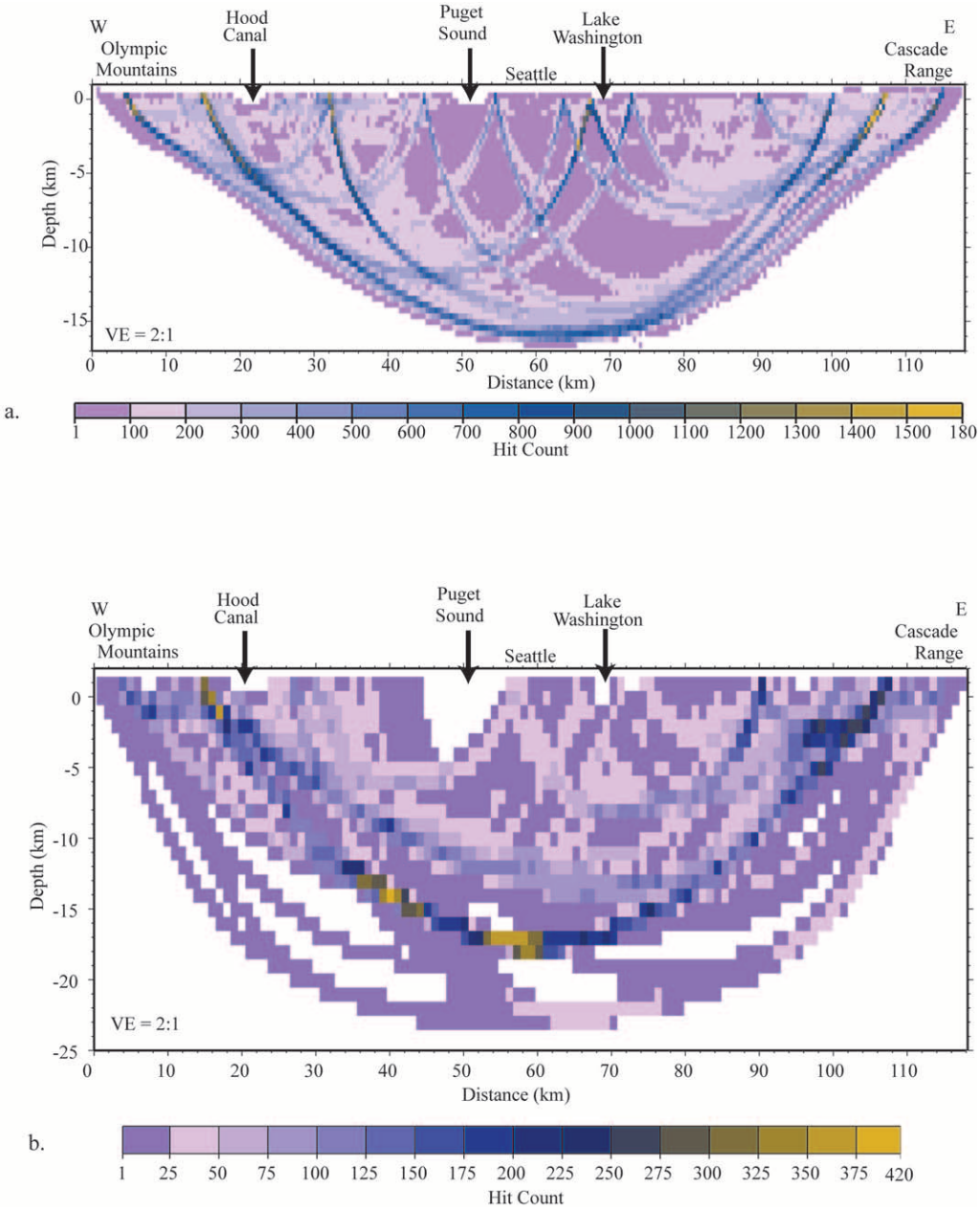

Figure 4. (a) Number of rays intersecting each cell (400 m square) for the 1999 SHIPS *P*-wave model. The minimum number of rays intersecting each cell is 5 and the maximum is 1884. (b) Number of rays intersecting each cell (1 km square) for the 1999 SHIPS *S*-wave model. The minimum number of rays intersecting each cell is 5 and the maximum is 420.

Kingston well, the top of Crescent Formation is interpreted as basalt interbedded with siltstone, tuff, and conglomerate (Rau and Johnson, 1999), and these rocks correspond to the depth where seismic velocities reach 4.5 km/sec (ten Brink *et al.*, 2002). We therefore use the 4.5 km/sec velocity contour as a proxy for the top of the Crescent Formation and the bottom of the Seattle basin.

The maximum basin thickness in our model is close to that determined by ten Brink *et al.* (2002) and is similar to that inferred from the north-trending 1991 Washington refraction line intersecting our profile at 84 km (Fig. 1a) (Miller *et al.*, 1997). The combination of our results and the north–south profiles confirm that the basin is asymmetric in the north–south direction, but nearly symmetric in the east–west direction (Johnson *et al.*, 1994; Pratt *et al.*, 1997; Brocher *et al.*, 2001; ten Brink *et al.*, 2002).

The asymmetry of the Seattle basin in a north–south direction has been inferred to be the result of its formation in response to motion on the Seattle fault zone (Johnson *et al.*, 1994). Consistent with this hypothesis, documented up-

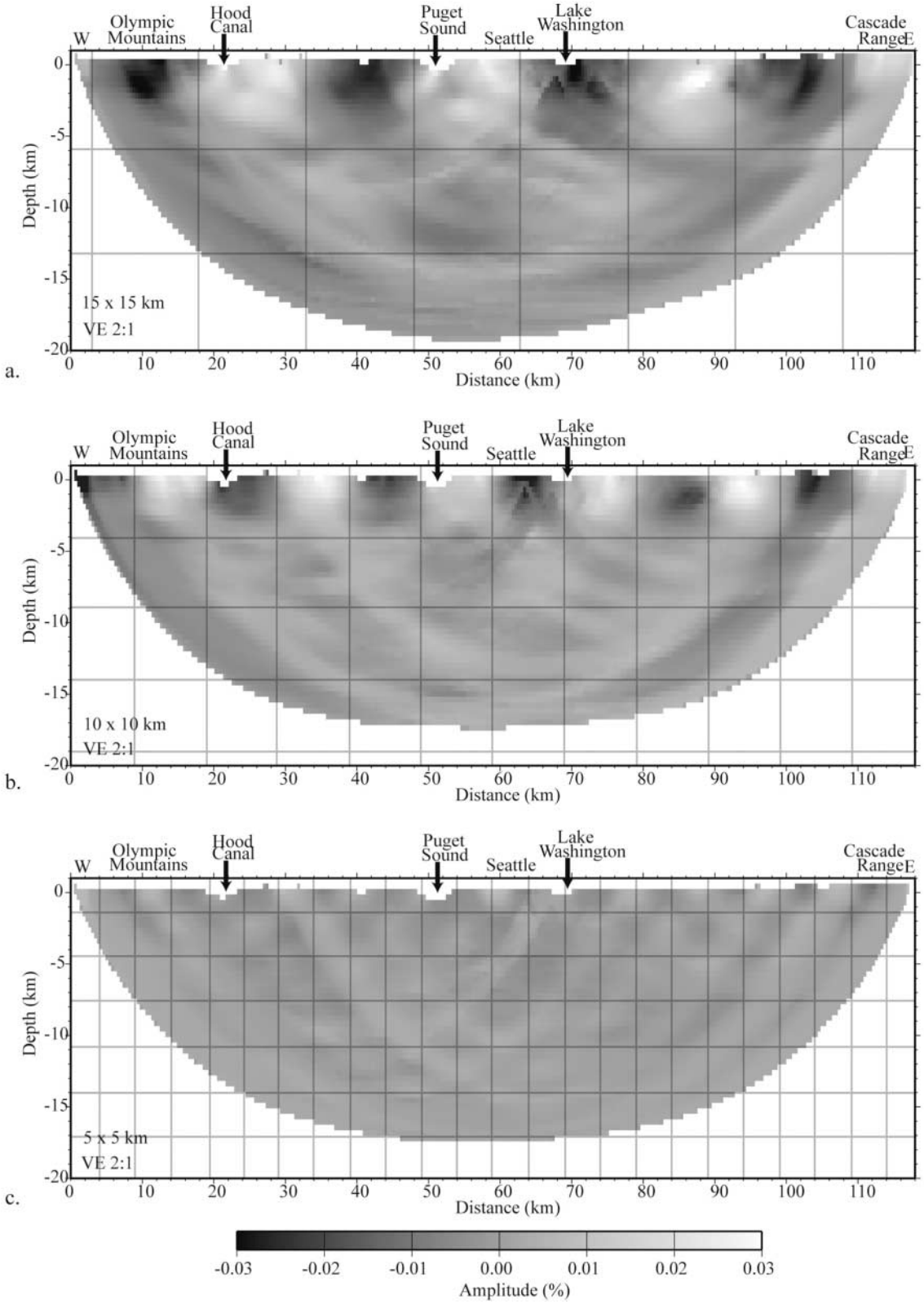

Figure 5. (a) 15 km × 15 km recovered checkers along the 1999 SHIPS *P*-wave profile at 3% amplitude. (b) 10 km × 10 km recovered checkers along the 1999 SHIPS *P*-wave profile. (c) 5 km × 5 km recovered checkers along the 1999 SHIPS *P*-wave profile.

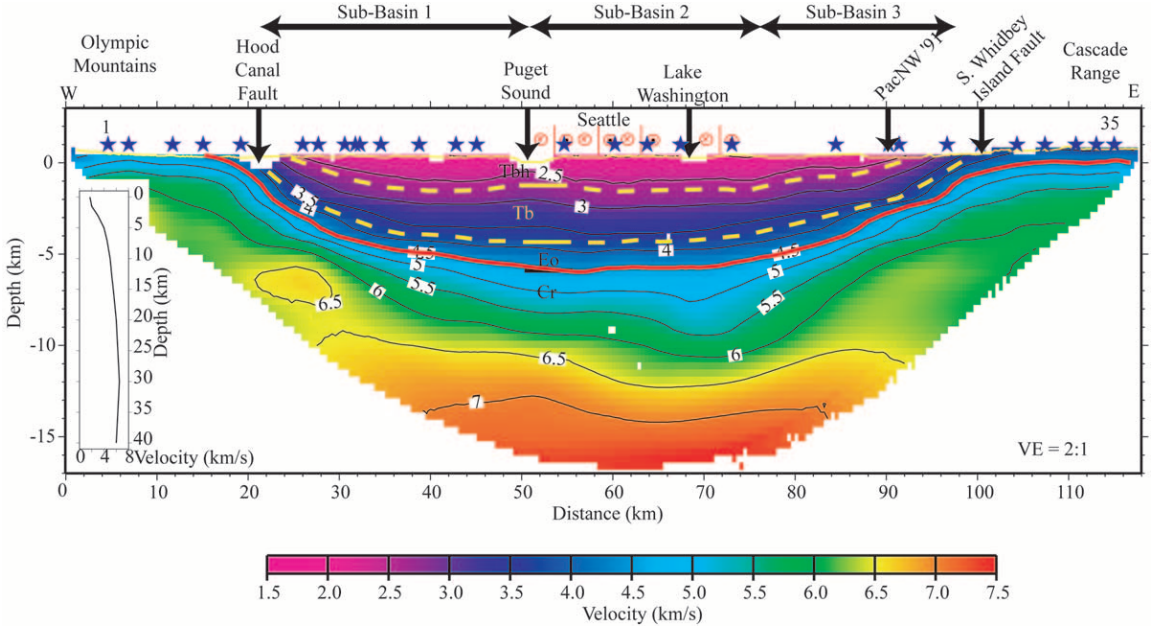

Figure 6. The 2D velocity model derived from the final *P*-wave velocity model with a contour interval of 0.5 km/sec. Inset is the initial 1D velocity used. Shot points are signified by blue stars. Surface elevation is represented by a yellow line. The 4.5 km/sec contour chosen as the base of the Seattle basin is highlighted in red. Major waterways along the profile are annotated. Yellow and black solid-line segments represent the stratigraphy from ten Brink *et al.* (2002) where their profile crosses the "Dry" SHIPS profile. The dashed yellow lines and solid red line are an interpretation following the velocity contours where these beds would continue in our model. The thin vertical red lines at the top of the model are locations of postulated strike-slip faults with sense of motion (Johnson *et al.*, 1999). The three subbasins are labeled at the top. Abbreviations: Blakely Harbor Formation, Tbh; Blakeley Formation, Tb; Eocene, Eo; Crescent Formation, Cr.

lift above the Seattle fault during Holocene earthquakes reaches a maximum near the center of the basin (Bainbridge Island), where high-resolution topography (Light Detection and Ranging, or LIDAR) have revealed the best evidence for surface faulting along the Toe Jam scarp (Nelson *et al.*, 2003). If the basin shape is indeed caused by the motion on the Seattle fault, the ~76-km width of the basin on our profile implies the Seattle fault is at least that length. The Seattle fault may be a few kilometers longer than the basin width imaged on our profile, because our profile is located about 5 km north of the Seattle fault zone and the width of the basin decreases northward (Brocher *et al.*, 2001, 2004).

Unconsolidated Deposits in the Seattle Basin

Unconsolidated deposits that are primarily Holocene and Quaternary, but that include older units, are defined on our profile based on their relatively low velocities (Fig. 6 and Ⓔ E1–E5 in the electronic edition of BSSA). The ten Brink *et al.* (2002) correlation with the Mobil-Kingston #1 well found that Quaternary and older unconsolidated units have velocities less than 2.5 km/sec. This correlation is also compatible with borehole logs (Brocher *et al.*, 2001). The average velocity of Pleistocene units in these well logs is 1.6 to 1.8 km/sec, but older unconsolidated deposits have velocities up to 2.4 km/sec.

Assuming that the 2.5 km/sec velocity contour represents the base of the unconsolidated deposits in our model, their thickness within the Seattle basin reaches up to 1 km along our profile (Fig. 6 and Ⓔ E1–E5 in the electronic edition of BSSA). Our estimated 1-km depth to the base of unconsolidated deposits in Puget Sound matches those of ten Brink *et al.* (2002) and Calvert *et al.* (2003), based on seismic-reflection profiles along the 1998 SHIPS transect and high-resolution seismic tomography. Our estimated thickness is ~2 times greater than that inferred solely from high-resolution seismic-reflection data (Frankel and Stephenson, 2000) and is thicker than that inferred by Jones (1996) from drill holes on nearby land and industry seismic-reflection data.

Shallow Subbasins within the Seattle Basin

Tomographic analysis of the 1998 SHIPS travel times suggest that the Seattle basin has several subbasins defined by closed velocity contours in map view (Brocher *et al.*, 2001). In cross section, there is evidence from our model for up to three subbasins, based on thickness variations of the

unconsolidated deposits (Fig. 6 and Ⓔ E1–E5 in the electronic edition of BSSA). Between Hood Canal and Puget Sound (beneath the Kitsap Peninsula) we identify a well-defined depression in the 2.5 km/sec contour that we label as subbasin 1. Between Puget Sound and 82 km (beneath Seattle and Redmond), there is another well-defined depression that we call subbasin 2. Between 72 and 80 km, near Lake Sammamish, we identify another, smaller depression that we labeled subbasin 3. A region of higher-velocity material beneath Puget Sound separates subbasins 1 and 2 and suggests that the base of the unconsolidated deposits may also be shoal. Because ground motions depend on the velocities within the shallow deposits, these subbasins may yield variations in ground motions during earthquakes as discussed in the following sections.

Tertiary Sedimentary Rocks in the Seattle Basin

In our tomography model, Eocene to Miocene sedimentary rocks have velocities between 2.5 and 4.5 km/sec (Fig. 6 and Ⓔ E1–E5 in the electronic edition of BSSA). At 52 km, where our model intersects the 1998 SHIPS seismic-reflection line (ten Brink *et al.*, 2002), the 3.8 km/sec velocity contour corresponds approximately to the interpreted bottom of the Oligocene Blakeley Formation. At this location velocities of less than 2.8 km/sec correspond approximately to interpreted Miocene Blakely Harbor Formation (Fig. 6 and Ⓔ E1–E5 in the electronic edition of BSSA), making this formation relatively thin on our profile. These estimates of *P*-wave velocities are close to those inferred from sonic logs, which show velocities for the Oligocene Blakeley Formation to vary between 2.4 and 3.6 km/sec and Eocene sedimentary rocks to have velocities between 2.8 and 4.0 km/sec (Brocher *et al.*, 2001).

Location of the Crescent/Cascadia Basement Contact

In the upper part of the basement rocks, at 60 km near Seattle, we identify a pronounced, eastward decrease in the vertical-velocity gradient at a depth of 6 km that we interpret as the change from Crescent Formation to pre-Tertiary Cascade basement rocks (Fig. 6 and Ⓔ E1–E5 in the electronic edition of BSSA). This decreased velocity gradient, which our checkerboard test suggests is well resolved, was also reported by Van Wagoner *et al.* (2002) on a nearby cross section parallel to ours and is consistent with lower velocities within the pre-Tertiary Cascade basement rocks compared with the Crescent Formation (Miller *et al.*, 1997). An east-trending refraction profile near ~46.5° E indicates that the Crescent/Cascade basement contact at the Mt. St. Helens seismic zone (SHZ, Fig. 1) is represented by a sharp eastward decrease in basement velocity (Parsons *et al.*, 1999). The contact is more subtle along our profile.

Our proposed location for the Crescent/Cascade basement contact near 60 km coincides with postulated north-trending strike-slip Eocene faults (Fig. 7) (Johnson, 1984, 1985; Johnson *et al.*, 1999) and with a vertical band of seismicity in the upper 5 km of the Seattle basin (Figs. 1a and 7). The depths of the seismicity could be speculative, but it could also indicate basement faulting extending into the sedimentary strata.

P-wave velocities increase with depth in the model, reaching a maximum of ~7.2 km/sec at 11 km depth. Velocities this high probably correspond to mafic members of the Crescent Formation volcanic rocks (Brocher and Christensen, 2001). An isolated high-velocity anomaly (>6.5 km/sec) on the west side of the model, just east of Hood Canal at a depth of 5 to 8 km, also may represent a more mafic component of the Crescent Formation (Figs. 6 and 7 and Ⓔ E1–E5 in the electronic edition of BSSA). However, the checkerboard tests reveal that below 7 km the model is not well resolved, and the velocities at the base of the model may therefore not be accurate.

S-Wave Velocity Model for the Seattle Basin

Our study provides the first detailed *S*-wave velocity model for the Seattle basin. As expected, the general features of our *S*-wave velocity model are similar to those of our *P*-wave velocity model. These similarities include the overall shape of the Seattle basin, the existence of shallow subbasins, and a high-velocity body beneath Hood Canal.

Our model shows *S*-wave velocities for Cenozoic sedimentary rocks within the basin ranging from 1 km/sec to 2.6 km/sec (Fig. 8 and Ⓔ E4 and E5 in the electronic edition of BSSA). Near-surface *S*-wave velocities within the basin are less than 1 km/sec in the west end of the basin (subbasin 1) increase to 1.3 km/sec in the center of the basin (subbasin 2), and decrease in the eastern end of the basin to 1.1 km/sec (subbasin 3; Fig. 8 and Ⓔ E4 and E5 in the electronic edition of BSSA). Although the *S*-wave velocity model may not show a "basin" shape in subbasin 2, we believe that the change in the velocity in the *S*-wave velocity model implies this change, but it is not as clear as the *P*-wave velocity model because of a lack of shallow *S*-wave ray coverage in this portion of the *S*-wave velocity model. The very near-surface velocities are consistent with recent shallow seismic measurements (e.g., Odum *et al.*, 2004). *S*-wave velocities for the Miocene Blakely Harbor Formation range to 1.7 km/sec; for the Oligocene Blakeley Formation, *S*-wave velocities vary from 1.7 to 2.0 km/sec; and for the Eocene sedimentary rocks, *S*-wave velocities range from 2.0 to 2.6 km/sec (Fig. 8 and Ⓔ E4 and E5 in the electronic edition of BSSA). *S*-wave velocities at the base of the Cenozoic sedimentary rocks filling the basin are close to 2.6 km/sec, corresponding to a V_p/V_s of 1.73 for the deep sedimentary strata.

S-wave velocities in the Crescent Formation volcanic basement rocks are substantially higher than those in the basin (Fig. 8 and Ⓔ E4 and E5 in the electronic edition of BSSA). Along the Olympic Peninsula, where Crescent Formation rocks crop out, *S*-wave velocities exceed 2 km/sec, even at the surface. Where the Crescent Formation is over-

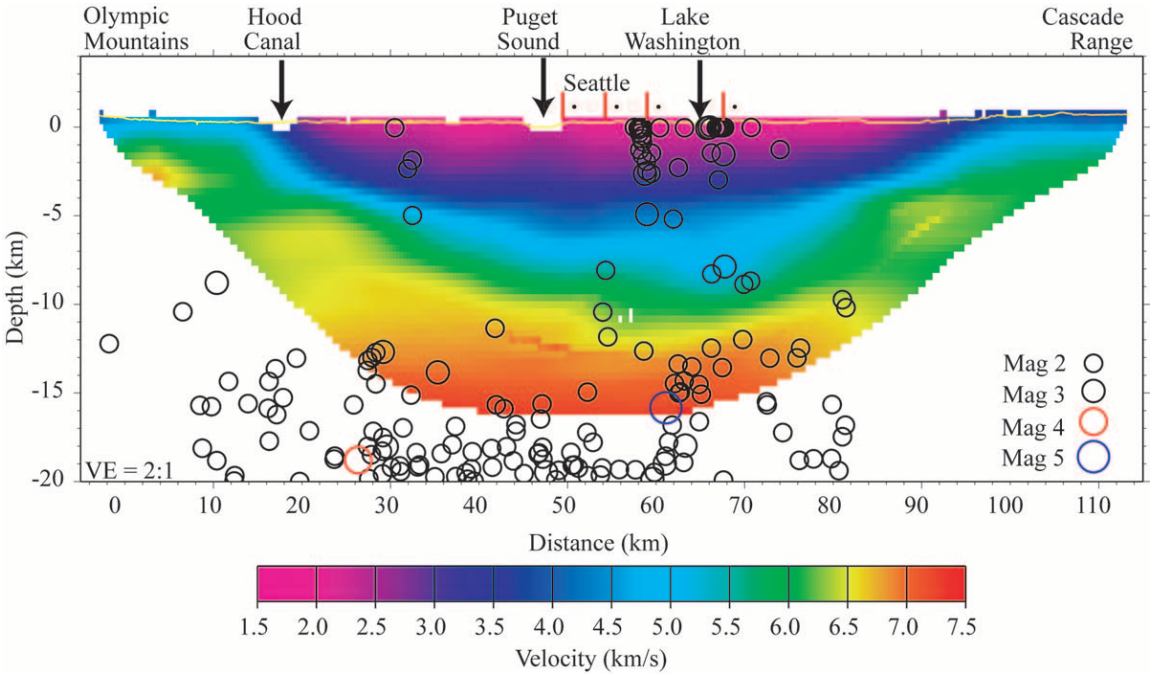

Figure 7. The 1999 SHIPS *P*-wave velocity model overlaid with local seismicity with epicenters within 5 km of the profile. The red lines are postulated strike-slip Eocene faults (Johnson *et al.*, 1999). A vertical band of seismicity in the upper 5 km of the Seattle basin near model km 70 coincides with the strike-slip faults and our proposed location for the Crescent/Cascade basement contact. The depth locations of this band of seismicity could be speculative, but it could also indicate basement faulting extending into the sedimentary strata. Events were compiled from the University of Washington catalog. A search width of 30 km from 1999 SHIPS east–west profile was used.

lain by a substantial sedimentary cover, our model indicates *S*-wave velocities near 2.6 km/sec at the top of the Crescent Formation, increasing to velocities of about 3.5 km/sec at depths of about 10 km, and to 4 km/sec at depths of 15 km at the center of the model. These velocities approximate the average V_s observed in the laboratory for 29 different samples of the Crescent Formation (Brocher and Christensen, 2001). Our *P*- and *S*-wave models yield V_p/V_s ratios of 1.71 to 1.81 for the Crescent Formation at depth, consistent with laboratory measurements of V_p/V_s (Brocher and Christensen, 2001).

Implications for Seismic Hazard and Crustal Structure

Comparison of Seattle Basin Geometry to Weak Ground Motions

Urban sedimentary basins, including the Seattle basin, represent a significant seismic hazard because of their tendency to amplify ground motions (Frankel *et al.*, 1999, 2002; Pratt *et al.*, 2003a; Barberopoulou *et al.*, 2004, 2006; Pratt and Brocher, 2006). Sedimentary basins beneath Los Angeles, Mexico City, and elsewhere amplify ground motions at the resonance period of the basins (Jongmans *et al.*, 1998; Wald and Graves, 1998). Amplification of strong ground motions around the edges of basins has been interpreted as resulting from interference patterns along crustal fault zones and thinning basins (Kawase, 1996; Graves *et al.*, 1998). Finally, surface waves generated within these basins are thought to be responsible for much of the increased amplitude and duration of shaking during earthquakes (Frankel *et al.*, 1999, 2002; Pratt *et al.*, 2003a; Barberopoulou *et al.*, 2004, 2006; Pratt and Brocher, 2006). A detailed understanding of basin geometry is critical for understanding and forecasting these phenomena (e.g., Frankel and Stephenson, 2000; Pitarka *et al.*, 2004). Our velocity models better characterize the Seattle basin geometry and can therefore be used to better assess the variations in ground motion expected for the basin.

As discussed earlier, the Seattle basin contains up to three shallow subbasins defined by local increases in the thickness of unconsolidated deposits (Figs. 6 and 8 and Ⓔ E1–E5 in the electronic edition of BSSA). Given the low shear- and compressional-wave velocities in these subbasins, their spatial distribution has importance for predicting lateral variations in site response.

Observations of weak ground motions in the Seattle basin during the 1999 SHIPS experiment indicate an amplification of the long-period motions (3- to 5-sec periods) by a

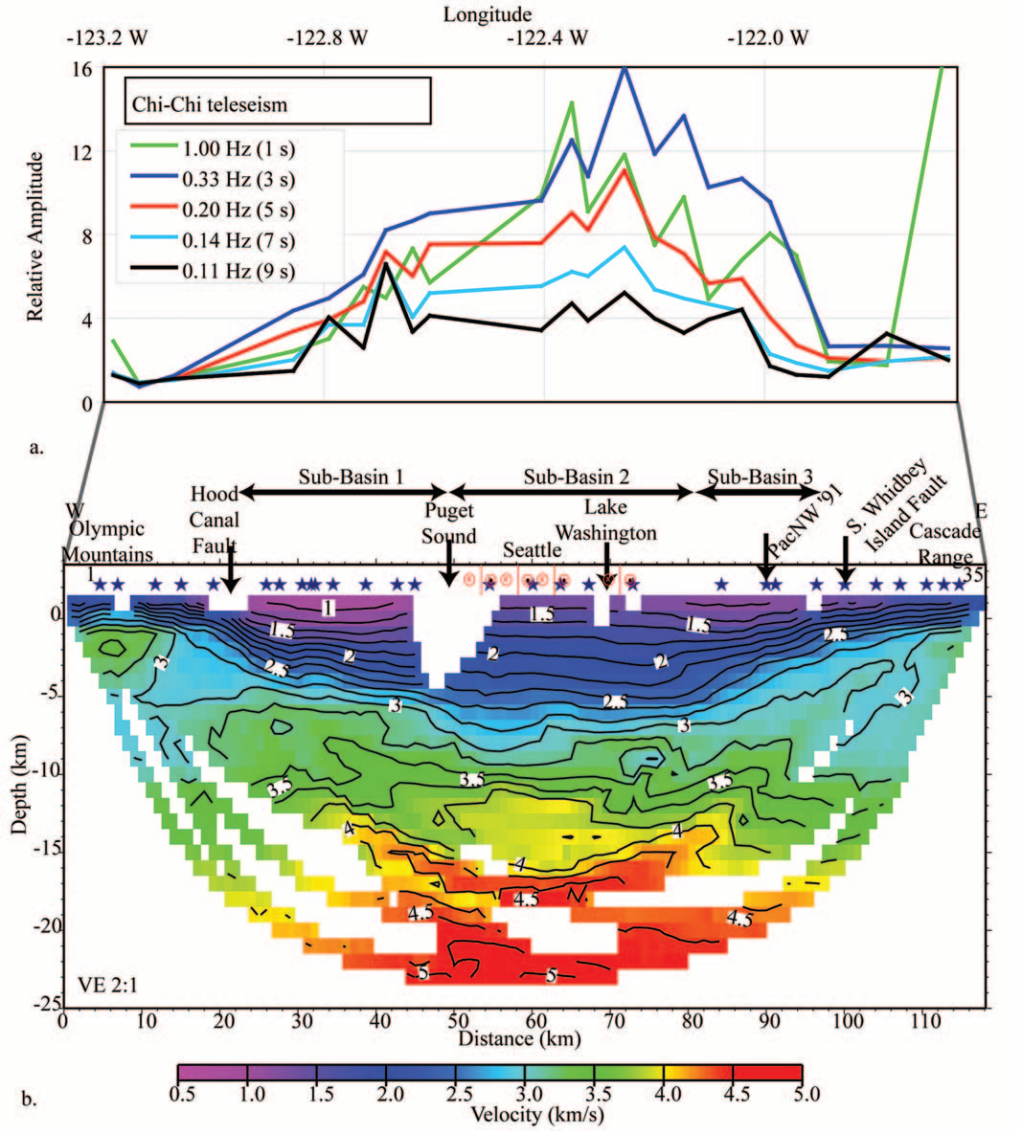

Figure 8. (a) Spectral amplitudes relative to bedrock sites at specific frequencies from Pratt *et al.* (2003a) aligned along the *x* axis with the *S*-wave model. (b) Shear-wave model along the 1999 SHIPS profile with a contour interval of 0.25 km/sec. Shotpoints are signified by blue stars. The red lines at the top of the model are locations of postulated strike-slip faults with sense of motion (Johnson *et al.*, 1999). The three subbasins from Figure 6 are labeled at the top. The high frequencies (1- to 5-sec periods) align with subbasins 2 and 3, which are highly faulted by the postulated strike-slip faults. Major faults and waterways along the profile are annotated.

factor of 10 or more relative to bedrock sites in the Olympic Peninsula (Fig. 8a) (Pratt *et al.*, 2003a). All frequencies below about 7 Hz show amplification, with the peak being about 0.33 Hz (3-sec periods). These observations were made using arrivals from the 1999 Chi-Chi, Taiwan earthquake, local earthquakes, and blasts recorded on a subset of our SHIPS seismometers, and therefore are coincident with the velocity models shown in Figures 6 and 8. We plot these amplification curves over the *S*-wave velocity model in Figure 8 to facilitate comparison of basin structure with amplification (Fig. 8a).

The primary observation is that at periods of 1 to 7 sec, the amplification curves are not symmetric across the basin but are skewed, with the largest amplifications occurring over the east-central part of the basin (near Lake Washington) (Fig. 8). From this asymmetry, we infer that the general basin geometry and overall thickness of Cenozoic sedimentary rocks is not the primary factor in controlling the observed weak ground motion amplification for periods of more than 1 sec. Instead, we note that the largest amplifications coincide with the thickest section of unconsolidated deposits in subbasin 2 near Lake Washington (Fig. 8a). Pratt

et al. (2003a) attributed most of the amplification to resonance in the shallow strata and to the generation of surface waves, both of which may correlate with the thickness and low velocity of unconsolidated deposits.

The largest amplifications lie east of the inferred Crescent/Cascadia basement contact at 60 km, above the pre-Tertiary Cascadia basement (Fig. 8). Hence, another possible contributor for this asymmetrical amplification is focusing by the Cascadia basement rocks (Pratt *et al.*, 2003a). Pratt *et al.* (2003a) performed forward modeling raytracing through a preliminary version of the *P*-wave velocity model shown in Figure 6 (the *S*-wave model was not yet available) and suggested that the overall basin geometry would lead to only 5 to 10% amplification of the arrivals. However, our *S*-wave velocity model shows a decrease in the velocities in the 10- to 15-km-depth range beneath subbasin 2, and this deep, low-velocity zone could focus *S*-wave energy into subbasin 2. Specifically, the *S*-wave arrivals from the Chi-Chi earthquake, which came from the west, could be refracted at the interface between the basement rocks, focusing energy toward the east side of the basin. Thus, it may be that a combination of thicker, slower near-surface deposits and focusing from deeper velocity anomalies cause the largest amplifications to occur in the east-central portion of the Seattle basin.

Pratt *et al.* (2003a) noted that at higher frequencies, at 7 Hz and above, intrinsic attenuation within the basin may damp out seismic energy and cause deamplification. This inference is supported by recent estimates of high intrinsic attenuation within the Seattle basin (Li *et al.*, 2006; Pratt and Brocher, 2006).

Finally, amplification curves for the 1999 Chi-Chi earthquake for periods between 7 and 9 sec exhibit greater symmetry and less amplification than for periods between 3 and 7 sec (Fig. 8). This greater symmetry of the long-period amplification mirrors the overall symmetry of the basin. Thus, we infer that at these long periods the overall basin geometry exerts an influence on the amplifications.

Other Seismic-Hazard Implications

As described earlier, the Seattle basin may have formed in response to motion on the Seattle fault, in which case the basin shape may be a proxy for the slip distribution of earthquakes on the Seattle fault (Johnson *et al.*, 1994; ten Brink *et al.*, 2002). This notion is supported by the fact that the thickest part of the basin, near Seattle, coincides with the best-developed Holocene fault scarps (Nelson *et al.*, 2003) and the largest land-level uplifts (Bucknam *et al.*, 1992). Our observation that the basin is at least 76 km long implies a fault of this length and a maximum magnitude of 7.2 for earthquakes on the fault zone assuming a down-dip extent of 20 km (Wells and Coppersmith, 1994).

The presence of shallow subbasins in the Seattle basin, with the boundary between the two major subbasins coinciding with hypothesized north–south faults and a change in location of the surface expression of the Seattle fault (Johnson *et al.*, 1999; Blakely *et al.*, 2002), raises the possibility that at least the uppermost parts of the Seattle fault zone are segmented. Brocher *et al.* (2004) interpret the Seattle fault zone as a passive roof duplex, with a north-vergent triangle zone bounded above by a shallow roof thrust. Segmentation of the roof thrusting may explain our observations of subbasins, and we note that such segmentation does not require segmentation of the master floor thrust inferred by Brocher *et al.* (2004).

Crescent Terrane/Cascadia Basement Contact

Interpretations of seismic-refraction profiles in the Cascades (Miller *et al.*, 1997) and near Mount Saint Helens (Parsons *et al.*, 1999) suggest that reduced velocity gradients in the upper part of the basement rocks near Seattle (60 km along the model) mark the contact between the Crescent Formation and pre-Tertiary Cascade basement rocks. To the north of the Seattle basin, the Southern Whidbey Island fault has been proposed to form this contact (Johnson *et al.*, 1996), and Blakely *et al.* (2004) summarized evidence for aeromagnetic and LIDAR topographic lineations along the southeastern projection of the Southern Whidbey Island fault to the north of our transect. Placing the contact between the Crescent Formation and pre-Tertiary Cascade basement rocks at 60 km in the model would require either a sharp southerly bend in any possible southeastern extension of the Southern Whidbey Island fault not observed in the aeromagnetic lineations (Blakely *et al.*, 2004), or it would require the contact to have formed along a different fault in this location (Johnson, 1984, 1985). Seismicity along the profile better supports the latter interpretation as it lines up with the lower-velocity gradient near Seattle and coincides at the surface with the location of a proposed north-trending strike-slip fault (Fig. 6 and Ⓔ E1–E5 in the electronic edition of BSSA) (Johnson *et al.*, 1994, 1999).

Tectonic Implications

The mild asymmetry of the Seattle basin, with a western end that dips more steeply than the eastern end, could have resulted from uplift of the Olympic Mountains in response to growth of the accretionary wedge (Brandon and Calderwood, 1990; Brandon and Vance, 1992). Uplift would have been produced by underthrusting of the Olympic core complex beneath the Crescent Formation, which resulted in flexure of the Crescent Formation on the west side of the Puget Lowland (Crosson and Symons, 2001). The west edge of the basin may therefore be controlled by a combination of motion on the Seattle fault and flexure caused by the underthrusting. Flexure of the Crescent Formation locally may, in part, be responsible for diffuse crustal seismicity at 20 to 30 km depth beneath Puget Lowland, but the overriding north–south compression is due to the oblique nature of the subduction (e.g., Van Wagoner *et al.*, 2002).

Summary

The 3D tomographic velocity models for the first time define the *P*- and *S*-wave velocity structure of the eastern end of the Seattle basin. The basin is broadly symmetric in the east–west section and reaches a maximum thickness of 6 km along our profile beneath north Seattle. The Seattle fault is estimated at 76-km length based on the *P*-wave velocity model, and the base of the basin is defined by the 4.5 km/sec contour in the *P*-wave velocity model. In addition, on the basis of closed velocity isocontours, the upper basin can be divided into three subbasins, which may each trap and amplify ground motions by different amounts. Comparison of our *S*-wave velocity model with coincident amplification curves suggests that the distribution of Quaternary deposits and reduced velocity gradients in the upper part of the basement east of Seattle have significance in forecasting variations in seismic-wave amplification across the basin. In particular, eastward increases in the amplification of 0.2- to 5-Hz energy correlate to locally thicker unconsolidated deposits and a change from Crescent Formation basement to pre-Tertiary Cascadia basement, although the direction of propagation may have also contributed to the asymmetric distribution of ground motions at these frequencies. This change, and a potential vertical band of seismicity along the profile, line up with postulated strike-slip faults. The correlation of subbasins, possible strike-slip faults, and the basement contact with the stronger amplification on the east side of the Seattle basin is clear evidence that the eastern portion of the Seattle basin will have amplified long-period ground motions during future earthquakes.

Data Sources

Seismic data can be obtained at the IRIS Data Management Center (http://www.iris.edu/about/DMC/).

Acknowledgments

This work was supported by the USGS Urban Geological Hazards Initiative and by external grants from the USGS National Earthquake Hazards Reduction Program to Oregon State University, the University of Texas El Paso (project 99HQGR0054), and the University of Washington. The instruments were provided by the Geological Survey of Canada and the PASSCAL facility of the Incorporated Research Institutions for Seismology (IRIS) through the PASSCAL Instrument Center at New Mexico Tech. Data collected during this experiment are available through the IRIS Data Management Center (http://www.iris.edu/about/DMC/). The facilities of the IRIS Consortium are supported by the National Science Foundation under Cooperative Agreement EAR-0004370. We thank the Washington State Departments of Forestry and Parks and Recreation, Olympic National Forest, the Bureau of Land Management, Kitsap and King Counties, and the cities of Bainbridge Island, Seattle, and Redmond for permission to access land under their jurisdiction. We thank the Weyerhaeuser Corp., International Paper Co., and numerous property owners for permission to access their land. Tom Burdette, USGS, organized and arranged permits for the fieldwork. We thank all those who helped to survey the lines, deploy and retrieve the recorders, and load and detonate the shots. Database and computational support was provided by the Pan American Center for Earth and Environmental Studies, which is supported by NASA. Seismic processing was conducted under the Landmark University Grant. We thank Shirley Baher, Aggeliki Barberopoulou, and Brett McLaurin for their early reviews of this article. In addition, we thank John Hole and Kumar Ramachandran for their reviews for the *Bulletin*.

References

Atwater, B. F., and A. L. Moore (1992). A tsunami about 1000 years ago in Puget Sound, Washington, *Science* **258,** 1614–1617.

Atwater, T. M. (1989). Plate tectonic history of the northeast Pacific and western North America, in *The Northeastern Pacific Ocean and Hawaii*, E. L. Winterer (Editor), *The Geology of North America*, Vol. N, Geological Society of America, 21–72.

Barberopoulou, A., A. Qamar, T. L. Pratt, K. C. Creager, and W. P. Steele (2004). Local amplification of seismic waves from the Denali earthquake and damaging seiches in Lake Union, Seattle, Washington, *Geophys. Res. Lett.* **31,** L03607, doi 10.1029/2003GL018569.

Barberopoulou, A., A. Qamar, T. L. Pratt, and W. P. Steele (2006). Long-Perios effects of the Denali earthquake on water bodies in the Puget Lowland: observations and modeling, *Bull. Seism. Soc. Am.* **96,** 519–535.

Blakely, R. J., B. L. Sherrod, R. E. Wells, C. S. Weaver, D. H. McCormack, K. G. Troost, and R. A. Haugerud (2004). The Cottage Lake Aeromagnetic Lineament: a possible onshore extension of the southern Whidbey Island fault, Washington, *U.S. Geol. Surv. Open-File Rept. 2004-1204*, 61 pp. http://pubs.usgs.gov/of/2004/1204 (last accessed July 2007).

Blakely, R. J., R. E. Wells, C. S. Weaver, and S. Y. Johnson (2002). Location, structure, and seismicity of the Seattle fault, Washington: evidence from aeromagnetic anomalies, geologic mapping, and seismic-reflection data, *Geol. Soc. Am. Bull.* **114,** 169–177.

Booth, D. B. (1994). Glaciofluvial infilling and scour of the Puget Lowland, Washington, during ice-sheet glaciation, *Geology* **22,** 695–698.

Brandon, M. T., and A. R. Calderwood (1990). High-pressure metamorphism and uplift of the Olympic subduction complex, *Geology* **18,** 1252–1255.

Brandon, M. T., and J. A. Vance (1992). Tectonic evolution of the Cenozoic Olympic subduction complex, Washington State, as deduced from fission track ages for detrital Zircons, *Am. J. Sci.* **292,** 565–636.

Brocher, T. M., and N. I. Christensen (2001). Density and velocity relationships for digital sonic and density logs from coastal Washington and laboratory measurements of Olympic Peninsula mafic rocks and greywackes, *U.S. Geol. Surv. Open-File Rept. 01-264*, 39 pp.

Brocher, T. M., and A. L. Ruebel (1998). Compilation of 29 sonic and density logs from 23 oil test wells in western Washington State, *U.S. Geol. Surv. Open-File Rept. 98-249*, 41 pp.

Brocher, T. M., R. J. Blakely, and R. E. Wells (2004). Interpretation of the Seattle uplift, Washington, as a passive roof duplex, *Bull. Seism. Soc. Am.* **94,** 1379–1401.

Brocher, T. M., K. C. Miller, A. M. Tréhu, C. M. Snelson, T. L. Pratt, C. S. Weaver, K. C. Creager, R. S. Crosson, U. S. ten Brink, M. G. Alvarez, S. H. Harder, and I. Asudeh (2000a). Report for explosion and earthquake data acquired in the 1999 Seismic Hazards Investigation of Puget Sound (SHIPS), Washington, *U.S. Geol. Surv. Open-File Rept. 2000-318*, 85 pp. http://geopubs.wr.usgs.gov/open-file/of00-318/ (last accessed July 2007).

Brocher, T. M., T. Parsons, R. A. Blakely, N. I. Christensen, M. A. Fisher, and R. E. Wells, and the SHIPS Working Group (2001). Upper crustal structure in Puget Lowland, Washington: results from 1998 Seismic Hazards Investigation in Puget Sound, *J. Geophy. Res.* **106,** 13,541–13,564.

Brocher, T. M., T. L. Pratt, K. C. Creager, R. S. Crosson, W. P. Steele, C. S. Weaver, A. D. Frankel, A. M. Tréhu, C. M. Snelson, K. C. Miller, S. H. Harder, and U. S. ten Brink (2000b). Urban seismic

experiments investigate Seattle fault and basin, *EOS Trans. AGU* **81,** 545, 551–552.

Brocher, T. M., T. L. Pratt, G. D. Spence, M. Riedel, and R. D. Hyndman (2003). Wide-angle seismic recordings from the 2002 Georgia Basin Geohazards Initiative, Northwestern Washington and British Columbia, *U.S. Geol. Surv. Open-File Rept. 03-160*, 34 pp. http://geopubs.wr.usgs.gov/open-file/of03-160/ (last accessed July 2007).

Brocher, T. M., T. L. Pratt, C. S. Weaver, C. M. Snelson, and A. D. Frankel (2002). Seismic recordings from the 2000 Kingdome Seismic Hazards Investigation in Puget Sound (SHIPS), Washington, *U.S. Geol. Surv. Open-File Rept. 02-123*, 29 pp. http://geopubs.wr.usgs.gov/open-file/of02-123/ (last accessed July 2007).

Bucknam, R. C., E. Hemphill-Haley, and E. B. Leopold (1992). Abrupt uplift within the past 1700 years at southern Puget Sound, Washington, *Science* **258,** 1611–1614.

Burchfiel, B. C., D. S. Cowan, and G. A. Davis (1992). Tectonic overview of the Cordilleran orogen in the western United States, in *The Cordilleran Orogen: Conterminous U.S.*, B. C. Burchfiel, P. W. Lipman, and M. L. Zoback (Editors), *The Geology of North America*, Vol. G-3, Decade of North American Geology, Geological Society of America, Boulder, Colorado, 407–480.

Calvert, A. J., M. A. Fisher, S. Y. Johnson, T. M. Brocher, K. C. Creager, R. S. Crosson, R. D. Hyndman, K. C. Miller, D. Mosher, T. Parsons, T. L. Pratt, G. Spence, U. ten Brink, A. M. Trehu, and C. S. Weaver (2003). Along-strike variations in the shallow seismic velocity structure of the Seattle fault zone: evidence for fault segmentation beneath Puget Sound, *J. Geophys. Res.* **108,** 2005, doi 10.1029/2001JB001703, 14 pp.

Crosson, R. S., and N. P. Symons (2001). Flexural origin of the Puget basins: implications for the Seattle fault and Puget basin tectonics (abstract), *EOS Trans. AGU* **82,** no. 47, F856.

Daneš, Z. F., M. M. Bonno, E. Brau, W. D. Gilham, T. F. Hoffman, D. Johansen, M. H. Jones, B. Malfait, J. Masten, and G. O. Teague (1965). Geophysical investigation of the southern Puget Sound area, Washington, *J. Geophys. Res.* **70,** 5573–5580.

Finn, C. (1990). Geophysical constraints on Washington convergent margin structure, *J. Geophys. Res.* **95,** 19,533–19,546.

Fisher, M. A., A. J. Calvert, T. Parsons, R. E. Wells, T. M. Brocher, and C. S. Weaver, and the SHIPS Working Group (2000). Crustal structure from SHIPS seismic reflection data along a transect from the southern Puget Lowland north to the San Juan Islands, *EOS Trans. AGU* **81,** 878.

Frankel, A., and W. Stephenson (2000). Three-dimensional simulations of ground motions in the Seattle region for earthquakes in the Seattle fault zone, *Bull. Seism. Soc. Am.* **85,** 1251–1267.

Frankel, A., D. Carver, E. Cranswick, M. Meremonte, T. Bice, and D. Overturf (1999). Site response for Seattle and source parameters of earthquakes in the Puget Sound region, *Bull. Seism. Soc. Am.* **89,** 468–483.

Frankel, A. D., D. L. Carver, and R. A. Williams (2002). Nonlinear and linear site response and basin effects in Seattle for the M 6.8 Nisqually, Washington earthquake, *Bull. Seism. Soc. Am.* **92,** 2090–2109.

Gower, H. D., J. C. Yount, and R. S. Crosson (1985). Seismotectonic map of the Puget Sound region, Washington, U.S. Geol. Surv. Misc. Invest. Ser. Map I-1613, scale 1:250,000.

Graves, R. W., A. Pitarka, and P. G. Somerville (1998). Ground-motion amplification in the Santa Monica area: effects of shallow basin-edge structure, *Bull. Seism. Soc. Am.* **88,** 1224–1242.

Haugerud, R. A., D. J. Harding, S. Y. Johnson, J. L. Harless, C. S. Weaver, and B. L. Sherrod (2003). High-resolution lidar topography of the Puget Lowland, Washington—A bonanza for earth science, *GSA Today* **13,** 4–10.

Hiett, B. J. (2000). 3D geometry and velocity structure of the Tacoma basin, western Washington, *M.S. Thesis*, University of Texas at El Paso, 113 pp.

Hole, J. A. (1992). Nonlinear high-resolution three-dimensional seismic travel time tomography, *J. Geophys. Res.* **97,** 6553–6562.

Johnson, S. Y. (1984). Evidence for a margin-truncating transcurrent fault (pre-Late Eocene) in western Washington, *Geology* **12,** 538–541.

Johnson, S. Y. (1985). Eocene strike-slip faulting and nonmarine basin formation in Washington, in *Strike-Slip Deformation, Basin Formation, and Sedimentation*, K. T. Biddle and N. Christie-Blick (Editors), Spec. Pub. Soc. Econ. Paleontol. Mineral. 37, 283–302.

Johnson, S. Y., R. J. Blakely, W. J. Stephenson, S. V. Dadisman, and M. A. Fisher (2004). Active shortening of the Cascadia forearc and implications for seismic hazards of the Puget Lowland, *Tectonics* **23,** TC1011, doi 10.1029/2003TC001507, 27 pp.

Johnson, S. Y., S. V. Dadisman, J. R. Childs, and W. D. Stanley (1999). Active tectonics of the Seattle fault and central Puget Sound, Washington—implications for earthquake hazards, *Geol. Soc. Am. Bull.* **111,** 1042–1053.

Johnson, S. Y., C. J. Potter, and J. M. Armentrout (1994). Origin and evolution of the Seattle fault and Seattle basin, Washington, *Geology* **22,** 71–74.

Johnson, S. Y., C. J. Potter, J. M. Armentrout, J. J. Miller, C. Finn, and C. S. Weaver (1996). The southern Whidbey Island fault: An active structure in the Puget Lowland, Washington, *Geol. Soc. Am. Bull.* **108,** 334–354.

Jones, M. A. (1996). Thickness of unconsolidated deposits in the Puget Sound Lowland, Washington and British Columbia, *U.S. Geol. Surv. Water Res. Invest Rept. (WRIR) 94-4133*.

Jongmans, D., K. Pitilakis, D. Demanet, D. Raptakis, J. Riepl, C. Horrent, G. Tsokas, K. Lontzetidis, and P.-Y. Bard (1998). EURO-SEISTEST: determination of the geological structure of the Volvi Basin and validation of the basin response, *Bull. Seism. Soc. Am.* **88,** 473–487.

Kawase, H. (1996). The cause of the damage belt in Kobe: "The basin-edge effect," constructive interference of the direct S wave with the basin-induced diffracted/Rayleigh waves, *Seism. Res. Lett.* **67,** 25–34.

Khazaradze, G., A. Qamar, and H. Dragert (1999). Tectonic deformation in western Washington from continuous GPS measurements, *Geophys. Res. Lett.* **26,** 3153–3156.

Lees, J. M., and R. S. Crosson (1990). Tomographic imaging of local earthquake delay times for three-dimensional velocity variation in western Washington, *J. Geophys. Res.* **95,** 4763–4776.

Li, Q., W.S.D. Wilcock, T. L. Pratt, C. M. Snelson, and T. M. Brocher (2006). Seismic attenuation structure of the Seattle basin, Washington State, from explosive-source refraction data, *Bull. Seism. Soc. Am.* **96,** no. 2, 553–571.

Miller, K. C., G. R. Keller, J. M. Gridley, J. H. Luetgert, W. D. Mooney, and H. Thybo (1997). Crustal structure along the west flank of the Cascades, western Washington, *J. Geophys. Res.* **102,** 17,857–17,873.

Monger, J.W.H., and W. J. Nokleberg (1996). Evolution of the northern North American Cordillera: generation, fragmentation, displacement, and accretion of successive North American plate-margin arcs, in *Geology and Ore Deposits of the American Cordillera*, A. R. Coyner and P. L. Fahey (Editors), Geological Society of Nevada, Reno, Nevada, 1133–1152.

Nelson, A. R., S. Y. Johnson, H. M. Kelsey, R. E. Wells, B. L. Sherrod, S. K. Pezzopane, L. A. Bradley, and R. D. Koehler, III (2003). Late Holocene earthquakes on the Toe Jam Hill fault, Seattle fault zone, Bainbridge Island, Washington, *Geol. Soc. Am. Bull.* **115,** 1388–1403.

Odum, J. K., W. J. Stephenson, K. Goetz-Troost, D. M. Worley, A. D. Frankel, R. A. Williams, and J. Fryer (2004). Shear- and compressional-wave velocity measurements from two 150-m-deep boreholes in Seattle, Washington, USA, *U.S. Geol. Surv. Open-File Rept. 2004-1419*, 36 pp. http://pubs.usgs.gov/of/2004/1419/OF2004_1419.pdf (last accessed July 2007).

Parsons, T., R. E. Wells, M. A. Fisher, E. Flueh, and U. S. ten Brink (1999). Three-dimensional velocity structure of Siletzia and other accreted terranes in the Cascadia forearc of Washington, *J. Geophys. Res.* **104,** 18,015–18,039.

Parsons, T., R. J. Blakely, and T. M. Brocher (2001). A simple algorithm for sequentially incorporating gravity observations in seismic travel-time tomography, *Int. Geol. Rev.* **43,** 1073–1086.

Pitarka, A., R. Graves, and P. Somerville (2004). Validation of a 3D velocity model of the Puget Sound regions based on modeling ground motion from the 28 February 2001 Nisqually earthquake, *Bull. Seism. Soc. Am.* **94,** 1670–1689.

Pratt, T. L., and T. M. Brocher (2006). Site response and attenuation in the Puget Lowland, Washington State, *Bull. Seism. Soc. Am.* **96,** 536–552.

Pratt, T. L., T. M. Brocher, C. S. Weaver, K. C. Miller, A. M. Tréhu, K. C. Creager, R. S. Crosson, and C. M. Snelson (2003a). Amplification of seismic waves by the Seattle basin, northwestern U.S., *Bull. Seism. Soc. Am.* **93,** 533–545.

Pratt, T. L., S. Johnson, C. Potter, W. Stephenson, and C. Finn (1997). Seismic reflection images beneath Puget Sound, western Washington State: the Puget Lowland thrust sheet hypothesis, *J. Geophys. Res.* **102,** 27,469–27,489.

Pratt, T. L., K. L. Meagher, T. M. Brocher, T. Yelin, R. Norris, L. Hultgrien, E. Barnett, and C. S. Weaver (2003b). Earthquake recordings from the 2002 Seattle Seismic Hazard Investigation of Puget Sound (SHIPS), Washington State, *U.S. Geol. Surv. Open-File Rept. 03-361*, 72 pp. http://geopubs.wr.usgs.gov/open-file/of03-361/ (last accessed July 2007).

Rau, W. W., and S. Y. Johnson (1999). Well stratigraphy and correlations, western Washington and northwestern Oregon, U.S. Geol. Surv. Geo. Invest. Ser. Map I-2621.

Riddihough, R. P. (1984). Recent movements of the Juan de Fuca plate system, *J. Geophys. Res.* **89,** 6980–6994.

Schultz, A. P., and R. S. Crosson (1996). Seismic velocity structure across the central Washington Cascade Range from refraction interpretation with earthquake sources, *J. Geophys. Res.* **101,** 27,899–27,915.

Schuster, R. L., R. L. Logan, and P. T. Pringle (1992). Prehistoric rock avalanches in the Olympic Mountains, Washington, *Science* **258,** 1620–1621.

Sherrod, B. L., T. M. Brocher, C. S. Weaver, R. C. Bucknam, R. J. Blakely, H. M. Kelsey, A. R. Nelson, and R. Haugerud (2004). Holocene fault scarps near Tacoma, Washington, USA, *Geology* **32,** 9–12.

Snelson, C. M. (2001). Investigating crustal structure in western Washington and in the Rocky Mountains: implications for seismic hazards and crustal growth, *Ph.D. Dissertation*, University of Texas at El Paso, 234 pp.

Symons, N. P., and R. S. Crosson (1997). Seismic velocity structure of the Puget Sound region from 3-D non-linear tomography, *Geophys. Res. Lett.* **24,** 2593–2596.

Tabor, J. J., and W. M. Cady (1978). The structure of the Olympic Mountains, Washington—analysis of a subduction zone, *U.S. Geol. Surv. Profess. Pap. 1033*, 38 pp.

ten Brink, U. S., P. C. Molzer, M. A. Fisher, R. J. Blakely, R. C. Bucknam, T. Parsons, R. S. Crosson, and K. C. Creager (2002). Subsurface geometry and evolution of the Seattle fault zone and the Seattle basin, Washington, *Bull. Seism. Soc. Am.* **92,** 1737–1753.

Van Wagoner, T. M., R. S. Crosson, K. C. Creager, G. F. Medema, L. A. Preston, N. P. Symons, and T. M. Brocher (2002). Crustal structure and relocated earthquakes in the Puget Lowland, Washington from high resolution seismic tomography, *J. Geophys. Res.* **107,** ESE 22-1–ESE 22-23, 2381, doi 10.10129/2001JB000710.

Wald, D. J., and R. W. Graves (1998). The seismic response of the Los Angeles basin, California, *Bull. Seism. Soc. Am.* **88,** 337–356.

Wells, D. L., and K. J. Coppersmith (1994). New empirical relationships among magnitude, rupture length, rupture width, rupture area, and surface displacement, *Bull. Seism. Soc. Am.* **84,** 974–1002.

Wells, R. E., C. S. Weaver, and R. J. Blakely (1998). Fore-arc migration in Cascadia and its neotectonic significance, *Geology* **26,** 759–762.

Zelt, C. A. (1998). Lateral velocity resolution from three-dimensional seismic refraction data, *Geophys. J. Int.* **135,** 1101–1112.

Department of Geoscience
University of Nevada Las Vegas
4505 Maryland Parkway, MS 4010
Las Vegas, Nevada 89154-4010
(C.M.S.)

U.S. Geological Survey
345 Middlefield Road, MS 977
Menlo Park, California 94025
(T.M.B.)

Department of Geological Sciences
University of Texas at El Paso
500 W. University Ave.
El Paso, Texas 79968
(K.C.M.)

U.S. Geological Survey
School of Oceanography
Box 357940
University of Washington
Seattle, Washington 98195
(T.L.P.)

College of Ocean and Atmospheric Sciences
Oregon State University
Corvallis, Oregon 97331
(A.M.T.)

Manuscript received 6 October 2005.